Wave load on submerged quarter-circular and semicircular breakwaters under irregular waves

Elsevier Editorial System(tm) for Coastal Engineering

Manuscript Draft

Manuscript Number: CENG-D-16-00008R2

Title: Wave load on submerged quartercircular and semicircular breakwaters under irregular waves

Article Type: Research Paper

Keywords: Submerged circular-front breakwaters; semicircular breakwater; quarter-circular breakwater; Wave load; RANS-VOF; Vorticity.

Corresponding Author: Dr. Qing-Ping Zou, Ph.D.

Corresponding Author's Institution:

First Author: xuelian jiang, Dr.

Order of Authors: xuelian jiang, Dr.; Qing-Ping Zou, Ph.D.; Na Zhang, Dr.

Abstract: Laboratory experiments were conducted to investigate the characteristics of wave loading on submerged circular-front breakwaters due to irregular waves. The wave force spectrum for a semicircular breakwater is similar to that for a quarter-circular breakwater. The peak wave force normalized by the incident wave height for irregular waves is less than that for regular waves. The performance of our theoretical wave load model is improved significantly by incorporating the effect of wave transmission and flow separation. A RANS-VOF model was used to investigate the effect of local hydrodynamic disturbances by submerged breakwaters on the pressure distribution around the breakwater and total wave load. The numerical results reveal that wave-induced vortex at the structure have a substantial influence on the wave loading on the submerged quarter-circular breakwater but not on the semicircular breakwater. A parametric analysis is used to further improve the relationship between the wave load and vortex.

***Highlights (for review)**

- Submerged quarter-circular and semicircular breakwaters have similar force spectra.
- Wave load under irregular waves is smaller than that under regular waves.
- Improved wave load model by incorporating wave transmission and flow separation and vortex effect.
- The effect of vorticity on the dynamic pressure is examined using RANS-VOF model.
- Correlation between vortex and wave load was found

Wave load on submerged quarter-circular and semicircular breakwaters under irregular waves

Xue-Lian Jiang[a, c], Qing-Ping Zou[bd*], Na Zhang[c]

[a] State Key Laboratory of Hydraulic Engineering Simulation and Safety, Tianjin University, 92 Weijin Road, Nankai District, Tianjin 300072, China,

[b] Department of Civil and Environmental Engineering, The University of Maine, 5711 Boardman Hall, Orono, ME 04469-5711, USA.

[c] Tianjin Key Laboratory of Soft Soil Characteristics & Engineering Environment, Tianjin Chengjian University, 26 Jinjing Road, Xiqing District, Tianjin 300384, China

[d] State Key Laboratory of Hydraulics and Mountain River Engineering, Sichuan University, 610065, Chengdu, China

* Corresponding author: qingping.zou@gmail.com

ABSTRACT: Laboratory experiments were conducted to investigate the characteristics of wave loading on submerged circular-front breakwaters due to irregular waves. The wave force spectrum for a semicircular breakwater is similar to that for a quarter-circular breakwater. The peak wave force normalized by the incident wave height for irregular waves is less than that for regular waves. The performance of our theoretical wave load model is improved significantly by incorporating the effect of wave transmission and flow separation. A RANS-VOF model was used to investigate the effect of local hydrodynamic disturbances by submerged breakwaters on the pressure distribution around the breakwater and total wave load. The numerical results reveal that wave-induced vortex at the structure have a substantial influence on the wave loading on the submerged quarter-circular breakwater but not on the semicircular breakwater. A parametric analysis is used to further improve the relationship between the wave load and vortex.

Keywords: *Submerged circular-front breakwaters; Irregular waves; Wave load model; Pressure; Vorticity.*

*Corresponding author.
E-mail address: qingping.zou@maine.edu (Q.-P. Zou).

1. Introduction

Breakwaters play an important role in mitigating wave damage and protecting shorelines from erosion. Traditionally, emerged breakwaters have been used for this purpose. However, designing emerged breakwaters has become increasingly difficult since the construction often takes place in a severe environment caused by fierce waves and a poor seabed [Mizutani et al., 1998; Jeng et al., 2013]. According to Rambabu and Mani [2005], submerged breakwaters have recently gained popularity in order to reduce pressures on the sheltered structures and retain sediments in the sheltered harbor through premature wave breaking [Burcharth et al., 2006]. In addition, submerged breakwaters provide more aesthetically pleasing view of the sea and better water quality in a harbor than emerged breakwaters [Johnson, 2006; Kobayashi et al., 2007].

Various types of submerged breakwaters have been employed in engineering practice, such as vertical, rubble mound, and circular-front breakwaters. They have different hydrodynamic performances due to the variation of wave reflection, dissipation, and transmission in response to the structure geometry. Young & Testik [2011] reported that semicircular breakwaters reflect less and transmit more energy than vertical breakwaters at the same relative submergence depth. Reduced wave reflection minimizes the seaside scour at the structure and benefits the navigation of vessels near the structure but greater wave transmission may deteriorate harbor tranquility and encourage beach erosion behind the structure. However, the submerged semicircular breakwaters with perforated walls may work well resulting in a smaller transmission coefficient because of additional energy dissipation by the turbulence inside the hollow chamber [Dhinakaran et al., 2009; Liu & Li, 2012]. Regarding wave loading, extensive studies on vertical breakwaters have been carried out in the past decades. Examples include the effect of wave breaker on dynamic pressures by Kirkgöz [1982, 1992], Ergin & Abdalla [1993], Hattori et al. [1994], Cooker & Peregrine [1992], Prabhkar & Sundar [2001], the influence of aeration and scale on wave impacts by Blackmore & Hewson [1984], Bullock et al. [2001, 2007], and dynamic response under wave attack by Oumeraci [1994], Franco [1994], Goda & Takagi [2000], Takahashi et al [2001], Li et al. [2006], Cuomo et al. [2011]. In comparison with vertical breakwaters, the pressure on a circular wall acts towards the center of the circle and therefore circular breakwaters generally have smaller horizontal

force, overturning moment and soil subgrade reaction [Tanimoto & Takahashi, 1994] that results in better stability and lower engineering cost [Dhinakaran et al., 2012].

This study focuses on the characteristics of wave loads on the circular-front breakwaters due to irregular waves. Two types of circular-front breakwaters have been used in coastal protection, i.e. quarter-circular breakwaters (QCB) and semicircular breakwaters (SCB). They consist of a curved concrete caisson founded on a rubble mound (see figure 2). At low water levels, circular breakwaters act as a rubble mound breakwater while serve as a composite breakwater at high water levels.

Since the first SCB was constructed at Miyazaki Port in Japan in 1993, efforts have been dedicated to characterize the dynamic pressure on SCBs. In summary, three wave load models for SCBs have been proposed. First in Tanimoto et al [1987], Goda's formulation for vertical breakwaters was modified by incorporating the phase and center angle difference to calculate the pressures on semicircular breakwaters. More wave energy will pass over submerged structures than emerged structures and therefore generate substantial surface fluctuation on the leeside, which can significantly alter the total wave loads. Yu et al. [1999] indicated that irregular wave forces on submerged SCBs exhibit very different behaviors from those on emerged SCBs. Xie [1999] concluded that submerged semicircular structures may be at risk if Tanimoto's formula was used in design. Instead, he proposed the second wave load model accordingly by including a pressure distribution on the inside circumference of the rear wall and introducing a new phase modification coefficient in Tanimoto's model. Yuan and Tao [2003] presented the third wave load model to predict the total wave forces on submerged, alternately submerged, and emerged SCBs based on a potential flow model. Figure 1 shows the freeboard ranges that these models can be applied [Li et al., 2003]. More discussions about the dynamic pressure on SCBs exposed to normally incident and oblique waves can be found in Sundar & Ragu [1997, 1998], Zhang et al. [2005] and Liu & Li [2013], respectively.

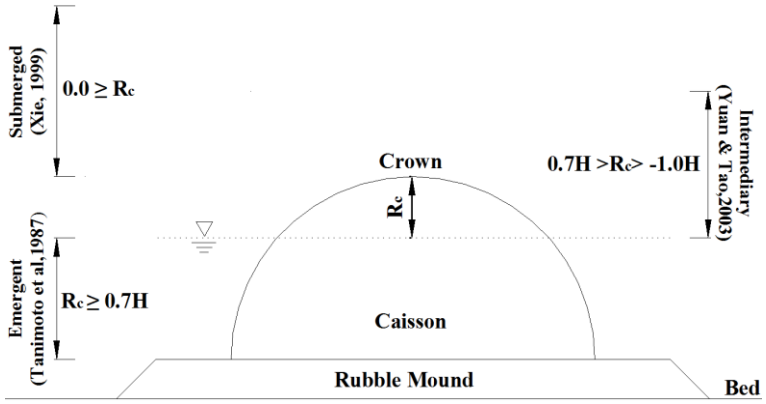

Figure 1. The valid range of freeboard of the empirical wave load models for semicircular breakwaters. R_c is crest freeboard height.

Xie et al. [2006] introduced the concept of QCBs based on SCBs in order to cut the construction cost since the bulk volume of QCBs is smaller than SCBS at a given crest height,. Literature on wave loads exerted on QCBs is rare. Xie et al. [2006] estimated the regular wave loads on QCBs by adding an amplification factor to Tanimoto's model for SCBs. Liu et al. [2006] discussed the effects of wave steepness, relative wave height, and water depth on the regular wave forces acting on QCBs. However, the irregular wave loads on QCBs have not been investigated previously.

Shi et al. [2011] found that with the same curved front wall, emerged QCBs and SCBs have the same hydrodynamic performance and wave loading. However, when a coastal structure is submerged, the presence of the structure changes the flow field adjacent to the structure for example, the generation and shedding of vortices around the structure [Young et al., 2009]. These vortices are expected to cause the oscillation of forces on submerged structures that cannot be neglected in design [Poupardin et al., 2012]. The intensity of vortex would depend on the wave parameters and structure geometry. Jiang et al. [2012] reported that submerged QCBs have greater energy dissipation than submerged SCBs partly due to stronger trailing vortices. It is therefore necessary to examine the effect of vortex dynamics on wave loads.

The main objective of this study is to improve the wave load model for submerged circular-front breakwaters exposed to irregular waves, and to examine the influence of wave-induced vortices on dynamic pressure. Firstly, the experimental setup is described

in section 2. Then, the characteristics of wave loads due to irregular waves are discussed in section 3. Subsequently, the predictions of a previous wave load model are compared with the measurements in section 4 and an improved model is proposed in section 5. In section 6, the effect of transmission on wave loads is further examined based on the measured pressure distributions and RANS-VOF modeling results of vortex dynamics. Finally, some concluding remarks are summarized in section 7.

2. Experiment Set-up

This experiment was carried out in the wave flume of the State Key Laboratory of Hydraulic Engineering Simulation and Safety at Tianjin University in China. The flume is 35 m long, 0.5 m wide and 0.8 m deep. At the inlet, a wave generator with perforated absorbers is used to produce desired incident waves. At the outlet, a permeable beach with a 1:4 slope is used to absorb the incoming wave energy. Structures were placed 20 m away from the wave generator to minimize the secondary reflection. The experiment configuration is shown in figure 2.

The test scale was set to 1:40 following geometric similarity, Froude law, and the wave conditions that can be generated in the flume. Impermeable concrete caissons of 0.15m in radius, 0.175m in height and the same width as the flume were erected on a rubble mound of 0.125m high filled with coarse gravel (see figure 2). The rubble mound has a seaward slope of 1:2 and a shoreward slope of 1:1.5.

The free surface displacement was measured using six wave gauges (gauge 1~gauge 6), as shown in figure 2 (a). The first three gauges were placed in front of structures for the wave reflection analysis. The distances among them were adjusted immediately before each run so that three-probe method for wave reflection analysis by Mansard and Funke [1980] can be applied. The fourth and fifth gauges were placed over the toe and heel of caissons to record the surface displacement near the caissons. The sixth gauge was one wavelength behind the structures to record the transmitted wave profile. The variation in pressure was measured by thirteen diaphragm-type pressure transducers fixed on the QCB and fourteen on the SCB (see figure 2 (b), P1~P14). All wave gauges and pressure transducers were calibrated immediately before each run to avoid zero drift. The same personal computer was used to provide the control signals to the wave generator

and acquire the signals from wave gauges and pressure transducers through an amplifier. During each run, data were recorded simultaneously from a 24-channel data acquisition card for 160 seconds at a sampling frequency of 50 Hz.

(a)

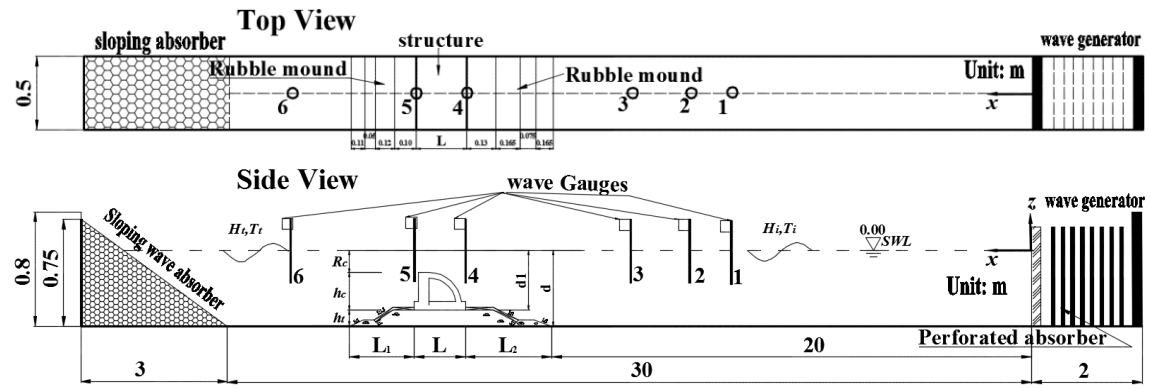

(b)

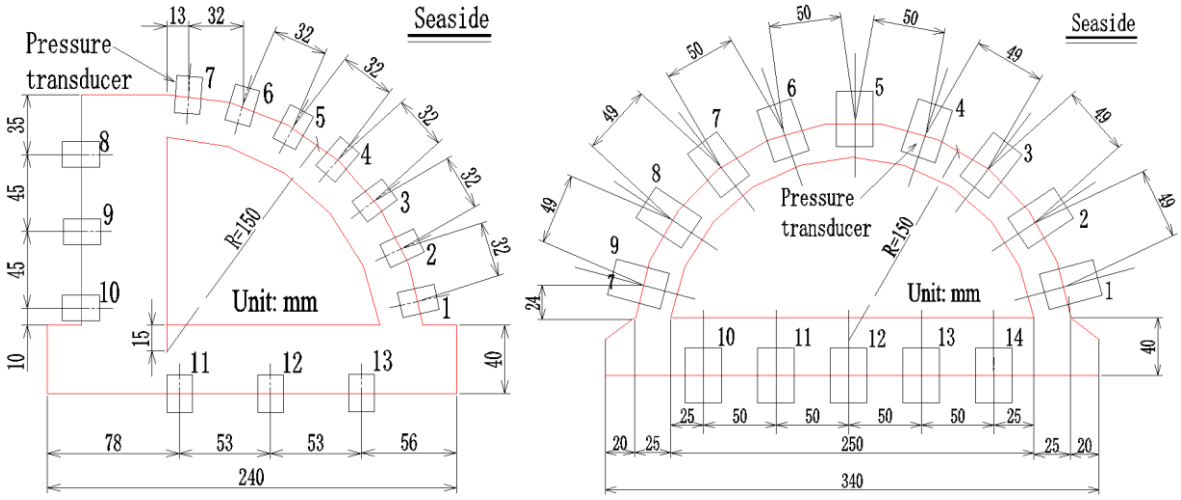

Figure 2. (a) Diagram of the experiment setup in the wave flume; (b) Pressure transducers on caissons.

Structures were subject to irregular waves defined by the JONSWAP-type spectra with a constant shape factor of γ =3.3. Significant wave heights in the range of 0.085m-0.117m and significant wave periods in the range of (1.24s-1.51s) were combined to generate the incident wave spectra. Tests 1-5 have a same period but different wave heights, while Tests 3 and 6-8 have a same wave height but different periods. During the entire set of tests, the water depth was set to 0.383 m representing the submerged condition. Table 1 lists the wave conditions for this experiment. To reduce the

error in measurements, each test was performed three times and the mean value was used in the analysis. The total number of runs was 24.

Table 1. Wave conditions.

Test No.	Significant wave height, H_s（m）	Significant wave period, T_s（s）	Peak wave period, T_p（s）	Significant wavelength, L_s（m）
Test-1	0.117	1.24	1.33	2.01
Test-2	0.100	1.24	1.33	2.01
Test-3	0.093	1.24	1.33	2.01
Test-4	0.085	1.24	1.33	2.01
Test-5	0.078	1.24	1.33	2.01
Test-6	0.093	1.44	1.54	2.45
Test-7	0.093	1.48	1.58	2.52
Test-8	0.093	1.51	1.61	2.59

To verify the performance of the wave generator and wave flume, a preliminary experiment was performed for all tests in Table 1 before structures were placed in the flume. Figure 3 exemplifies the time histories of the surface displacement and the incident spectrum. The agreement between the measured and desired wave spectra is very good except for small deviations at some frequencies.

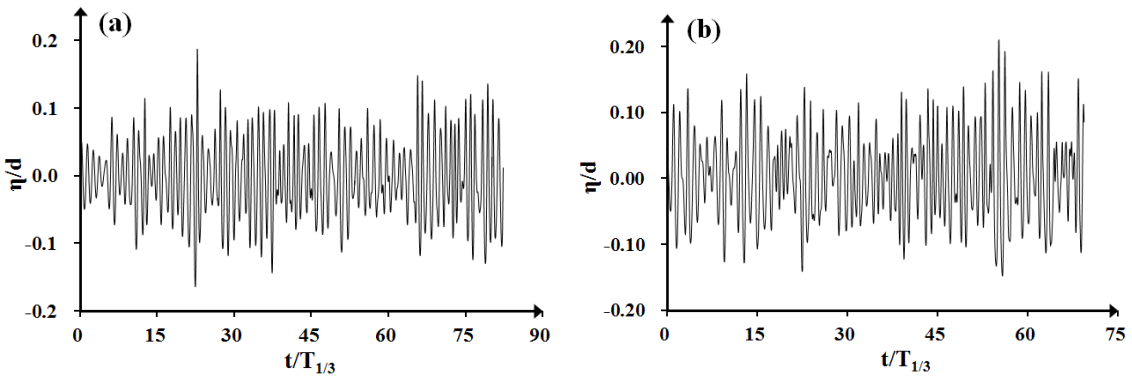

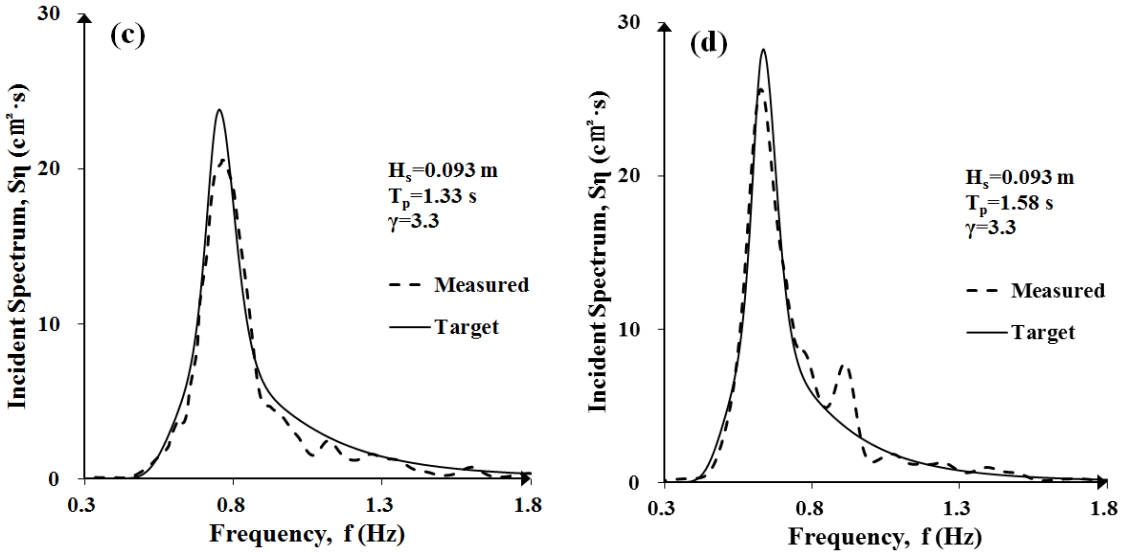

Figure 3. Time series of measured and desired wave elevation (a, b) and incident wave spectrum (c, d): (a) & (c) are for test 3 (d =0.383 m, H_s =0.093 m, T_p =1.33 s); (b) & (d) are for test 7 (d =0.383 m, H_s =0.093 m, T_p =1.58 s). η refers to the surface displacement and d refers to the water depth.

3. Experimental results

Caissons must be designed properly in order to sustain the potential sliding and overturning motions induced by waves. For circular-front caissons, the overturning moment is small, and hence the sliding failure is the major concern in its design. Oumeraci et al. (2001) pointed out the sliding failure of vertical breakwaters often takes place when the shoreward horizontal force reaches its peak. However, Rao et al. [2001] came to a different conclusion for the submerged SCBs that the sliding failure most likely occurs at the time of the maximum seaward horizontal force. Therefore, we will reexamine these findings in this study.

Figure 4 shows the time series of the horizontal force (F_h), the vertical force (F_v) and the safety margin against sliding (K_s). At each time step, the total wave forces are calculated by integrating the instantaneous pressure distribution along the surface of the structures using the Simpson rule (Polyanin and Manzhirov, 1998). Then, the total wave forces are decomposed into horizontal (F_h) and vertical components (F_v). F_h is positive

shoreward and F_v is positive upward. It should be noted that the vertical force (F_v) includes both the vertical component of pressures on the wall and the uplift pressure on the base of caissons. The safety margin against sliding is proposed by

$$K_s = \frac{f\left[\gamma_G G - \gamma_v F_v\right]}{\gamma_h F_h}, \tag{1}$$

where G is the weight of caissons in still water (0.493kN/m for the QCB and 0.551kN/m for the SCB), f =0.6 is the friction coefficient between the caisson and the rubble mound, γ_G =1.0, γ_v = 1.25, γ_h =1.25 are the partial safety factors to account for the uncertainties in G, F_v, F_h and their relative importance in the sliding failure. There is a phase shift between the horizontal and vertical forces, which is expected to change with the geometry of the breakwater relative to wavelength, freeboard and local water depth. The minimum safety margin against sliding ($K_{s\min}$) occurs at the peak shoreward horizontal force. The shoreward horizontal force ($F_{+h\max}$) plays a crucial role in the sliding instability of the submerged caissons. Hence, we will next focus on $F_{+h\max}$.

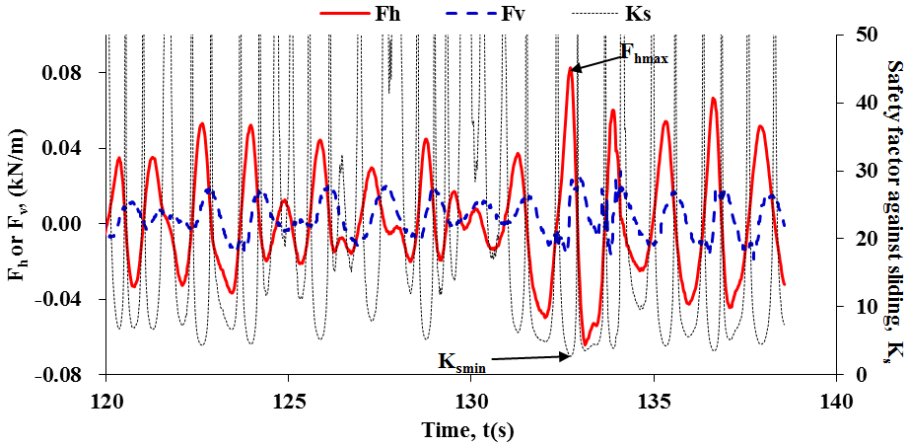

Figure 4. Typical time histories of the horizontal and vertical forces, and the safety margin against sliding for the quarter-circular breakwater (test 2: $d = 0.383\,m$, H_s = $0.10\,m$, $T_s = 1.24\,s$).

Figure 5 compares the spectra of the horizontal force on the QCB and on the SCB. It can be observed from figure 5 (a) that the force spectra exerted on the QCB is similar to

those of the SCB. This result implies that the wave load model for a submerged SCB can be applied to a submerged QCB. Moreover, the force spectra are similar to the incident wave spectra (see figure 3), which means little energy transference between higher and lower harmonies when waves pass over well-submerged structures. It also shows that the peak value of force spectra increases with wave height but decreases with wave period. Goda [1970] suggested a spectral peakedness parameter ($Q_p = \frac{2}{m_0^2}\int_0^\infty \omega S^2(\omega) d\omega$) to describe the peakedness of spectral peak and spectral width that correlates with wave groups and the corresponding damage to coastal structures. Figure 5(b) demonstrates the horizontal wave forces for the QCB and the SCB have a similar spectral profile to the incident wave. The spectral peakedness parameter of the horizontal force $(Q_p)_{Fh}$ increases linearly with that of the incident wave $(Q_p)_\eta$. On average, the spectral width for the QCB is 9% narrower than that for the SCB and 6% narrower than that for the incident wave.

In addition, the observed dimensionless maximum horizontal force for irregular waves in this study ($F_{h\max}/\gamma_w H_i R$, R refers to the radius of the circular wall) are compared with the observation of Liu et al. [2006] for regular waves. We found that the former is 20% for the SCB and 35% for the QCB smaller bthan the latter.

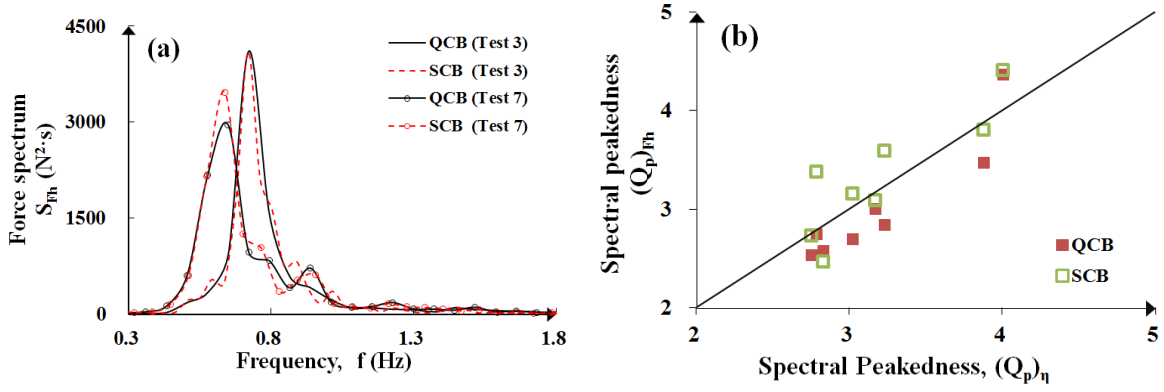

Figure 5. Spectral analysis: (a) Spectral density of the horizontal force (test 3: d =0.383 m, H_s =0.093 m, T_p =1.33 s; test 7: d =0.383 m, H_s =0.093 m, T_p =1.58 s); (b) Spectral peakedness parameters for the horizontal force and the surface displacement.

the diagonal line denotes equal spectral peakedness.

4. Model-data comparison

The results in Section 3 show that submerged quarter- and semi- circular breakwaters have a similar dynamic response to irregular waves. In this section, the predictions of a wave load model for submerged SCBs subject to regular waves are compared with the measurements of irregular waves.

As reviewed in the introduction, there are three wave load models for SCBs (see figure 1). Xie's model (1999) for submerged SCBs (see Appendix A) is adopted here since the structures were submerged during the entire test. First, we need to define design wave parameters. Goda [2010] suggested $H_{\max} = 1.8H_s$ and the Chinese Code of Hydrology for Sea Harbor defined $H_{1\%}$ as the design wave. Both recommendations have been tested in this study. Using $H_{1\%}$ .gives better agreement between model and data. Therefore, $H_{1\%}$ was chosen as the design wave in our calculation. The design wave period is taken as that of significant wave according to Goda [2010], i.e. $T_i = T_{1/3}$. Besides, it should be noted that caissons in this study are impermeable as classified in Sasajima et al. [1994], i.e. we substitute ε_b=0 in the equation (A.6) and p_0'=0 in the equation (A.7). Other parameters are specified in figure A-1.

Figure 6 shows that the ratio of Xie's (1999) model predictions to our measurements has a mean value of 1.15 and standard deviations of 0.18 for the QCB and 0.14 for the SCB. The mean value implies Xie's (1999) model overestimate the observed wave load. Sasajima et al. [1994] drawn the same conclusion about Tanimoto's model based on their field tests at a rear-perforated SCB constructed at Miyazaki Port in Japan. Figure 6 also shows that the ratio of the measured maximum horizontal forces on QCB and SCB is about 1.05, which is much lower than the value of 1.30 reported by Xie (2006) for regular waves. Thus, Xie's model is suitable for a deterministic design but not for irregular waves.

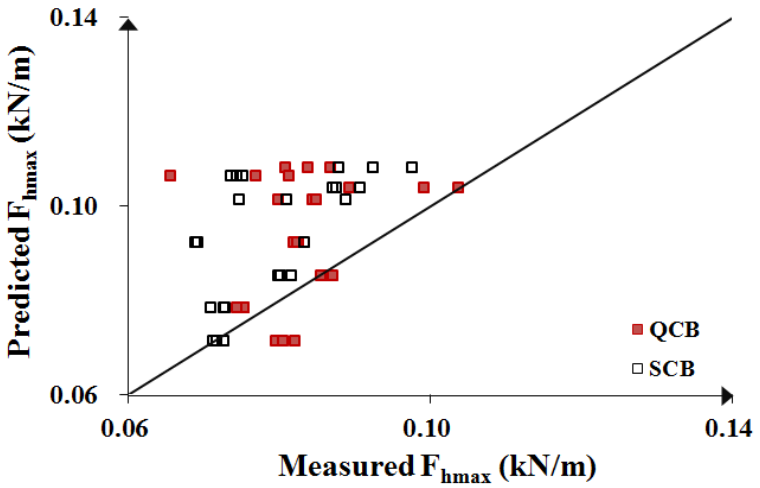

Figure 6. Comparison between the predicted maximum horizontal force by Xie's (1999) wave load model and measurements for the quarter- (solid square) and semi- (open square) circular breakwaters. The diagonal line represents the prediction is equal to the observation.

5. Improved wave load model

The wave load model by Xie (1999) was derived from Goda's formulation for vertical breakwaters with small overtopping and transmission. As a result, the larger waves on the seaside of structures cause a greater force on the front wall than the back wall, therefore, the contribution of the pressure on the rear wall is negligible. However, for a submerged structure, more incident wave energy is transmitted to the leeside and generates a larger wave behind the structure than an emerged one does. The transmitted wave is expected to cause a significant wave impact on the rear wall [van der Meer et al., 2005]. Figure 7 compares the percentage of contribution of the force components on the front $(F_h)_{front}$ and rear wall $(F_h)_{rear}$ to the maximum horizontal force ($F_{h\max}$). The average ratio $\frac{(F_h)_{front}}{F_{h\max}}$ is 72% and $\frac{(F_h)_{rear}}{F_{h\max}}$ is 28%. This result suggests that the contribution of pressures on the rear wall needs to be included in calculating the wave force on a submerged breakwater.

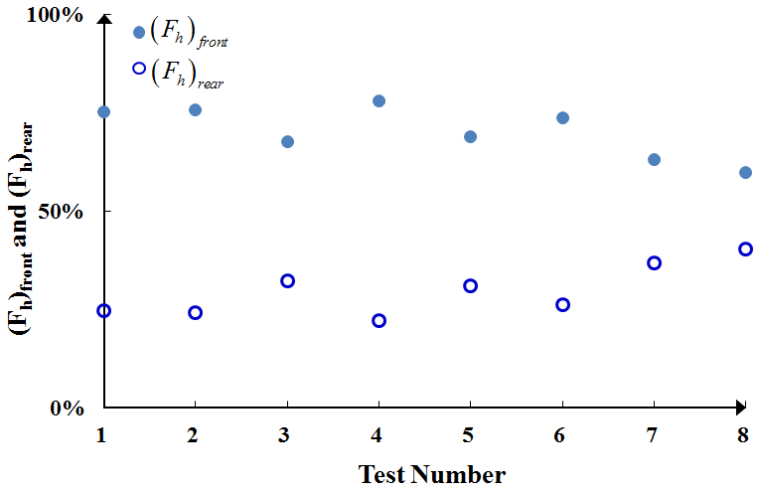

Figure 7. The percentage of contribution from the wave force acting on the front $\frac{(F_h)_{front}}{F_{h\max}}$ (solid circle) and rear wall $\frac{(F_h)_{rear}}{F_{h\max}}$ (empty circle) to the total peak horizontal force ($F_{h\max}$)=$(F_h)_{front}+(F_h)_{rear}$ for the quarter-circular breakwater.

We will next extend Xie's model (See Appendix A) by including the effect of wave transmission and form drag due to the wake behind the structure on the wave loads over submerged circular breakwaters. As listed in table 1, eight test cases were conducted in the experiment and each case was repeated three times. The measurements in tests 1, 3, 5 and 7 representing various wave conditions were used to derive the correction coefficients (2 runs in each case and 8 runs in total) and the other sixteen runs were used to verify the improved model. When waves encounter a submerged breakwater, the instantaneous force on the structure consists of the potential flow component mainly due to the free surface displacement and the form drag component due to the wake around the structure [Dean & Dalrymple, 1991]. Accordingly, the maximum horizontal force is given by

$$F_{h\max} = F_{hW} + F_{hD}, \tag{2}$$

where F_{hW} represents the potential component of horizontal force and F_{hD} represents the drag component.

In potential wave theory, pressures acting on a submerged structure mostly depend on the free surface displacement around the structure. The instantaneous surface

displacement in figure 8 shows that when the horizontal force reaches its peak, a wave crest is passing over the toe of caisson (recorded by gauge 4) and a surface elevation below the still water level is at the heel (recorded by gauge 5).

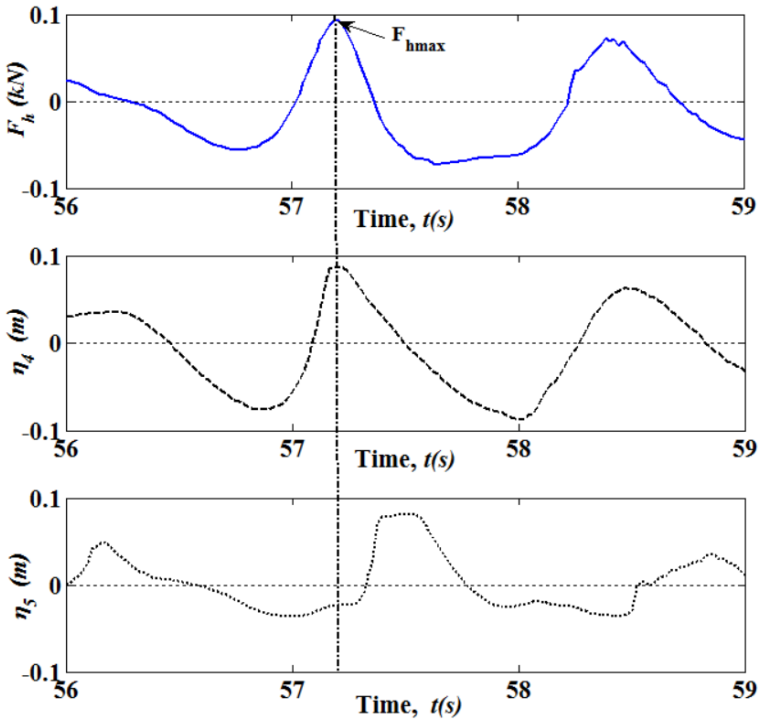

Figure 8. Time evolution of the horizontal wave force (upper panel) and surface displacements at gauge 4 (middle panel) and 5 (lower panel) for the semicircular breakwater (test 1: $d = 0.383\,m$, $H_s = 0.117\,m$, $T_p = 1.33\,s$). η_4 and η_5 are the surface displacement recorded by gauge 4 at the toe and gauge 5 at the heel of the caisson. The vertical dash dot line corresponds to the time of the maximum horizontal wave force.

Therefore, the surface displacement at the structure consists of the reflection and transmission components,

$$\eta_{h\max} = |\eta_r| + |\eta_t| . \tag{3}$$

The amplitude of surface elevation (η_r) due to reflection can be expressed as $|\eta_r| = 0.5\lambda_r (1+\cos\beta)\left(\alpha_1 + \alpha_2 \cos^2\beta\right) H_i$ based on the equation (A.2). The correction factor λ_r varies with the structure type (for upright walls, λ_r=1.0). The surface profile (η_t) due to transmission is related to the relative submerged depth ($\frac{R_c}{H_i}$) and the wave

breaking parameter (ξ_{p0}) (van der Meer et al., 2005), where R_c the freeboard, $\xi_{0p} = \tan\alpha \Big/ \sqrt{2\pi H_i / gT_p^2}$ the peak Iribarren parameter, $\tan\alpha$ the fictional slope connecting toe and crown (0.43 in this study), T_p the peak period of incident waves. We modify the expression by van der Meer et al. (2005) for wave transmission at smooth and impermeable low-crested structures as $|\eta_t| = \left\{ \lambda_{t1} \left(\frac{|R_c|}{H_i} \right)^{\lambda_{t2}} + \lambda_{t3} \left[1 - \exp\left(-0.5 \xi_{p0} \right) \right] \right\} H_i$ by including three correction coefficients λ_{t1}, λ_{t2}, λ_{t3}. Using the surface profile in equation (3), we rewrite the equation (A.2) for the pressure at still wave level as

$$\begin{aligned} p_s^{'} &= \gamma_w \eta_{h\max} \\ &= \left\{ 0.5\lambda_r \left(1+\cos\beta\right)\left(\alpha_1 + \alpha_2 \cos^2\beta\right) + \lambda_{t1} \left(\frac{|R_c|}{H_i} \right)^{\lambda_{t2}} + \lambda_{t3} \left[1 - \exp\left(-0.5 \xi_{p0} \right) \right] \right\} \gamma_w H_i . \end{aligned} \quad (4)$$

Correction coefficients in equation (4) have been tentatively estimated with the measurements by gauge 4 and gauge 5. We obtain λ_r =0.52, λ_{t1} =0.06, λ_{t2} =0.52, λ_{t3} =0.09 for the QCB, and λ_r =0.72, λ_{t1} =0.05, λ_{t2} =0.48, λ_{t3} =0.12 for the SCB.

The pressure at the bottom level of caisson ($p_b^{'}$) can be calculated by the equation (A.3)

$$p_b^{'} = p_b = \alpha_3 p_s^{'} . \quad (5)$$

The phase modification coefficient $\lambda_p^{'}$ in the equation (A.3) is neglected here in equation (5) for the following reasons. An assumption for the equation (A.3) is that the horizontal force should reach its peak value when a wave crest is passing over the crown of circular walls. As a result, the pressure at the toe of caisson ($p_b^{'}$) should be reduced due to a wave phase discrepancy between the toe and crown. However, in this study, we observed that the horizontal force reaches its peak value when a wave crest is passing over the toe instead of the crown of circular wall. For example, the pressure recorded by P1 near the toe (see figure 2) is close to its peak value because it is at the wave crest phase at this point. Meanwhile, the pressure acting on the other part of the front circumference is smaller than its peak value due to its phase lags from P1. Thus, we

obtain the expression for pressures acting on the front circumference by including the phase modification coefficient $\lambda_p^{'}$

$$p(\theta)=\left(\alpha_3-\alpha_3\frac{z}{d_1}+\frac{z}{d_1}\right)\lambda_p^{'}p_s^{'}\cos\theta\,, \tag{6}$$

where $p(\theta)$ pressure after angle correction, θ the central angle, d_1 the water depth above wall bottom, $\lambda_p^{'}$ the phase correction coefficient and z the vertical coordinate with z =0 located at the still water level and positive upward. Xie's model adopted $\lambda_p{}'=\cos\left[\frac{2\pi(\Delta l)'}{L_s}\right]$ based on the linear wave theory by neglecting the wave transformation over submerged structures, where $(\Delta l)'$ the horizontal distance between toe and crown, L_s the significant wavelength. Assuming $\lambda_p^{'}=\lambda_{p1}\cos\left(\lambda_{p2}\cdot\frac{2\pi(\Delta l)'}{L_s}\right)$, we obtain λ_{p1}=0.76, λ_{p2}=3.0 for the QCB and λ_{p1}=0.81, λ_{p2}=3.6 for the SCB based on the measurements of pressure on the front wall.

The potential flow component of horizontal force due to the free surface displacement is given by

$$F_{hW}=\int_{frontwall}p(\theta)\cos\theta dl\,. \tag{7}$$

The wave force F_{hW} calculated from equation (3) ~ (7) is the potential component of horizontal force rather than the total force $F_{h\max}$. It is in a good agreement with the measurement for the SCB but underestimate that for the QCB by 16%. The reason could be that the measured surface displacement $\eta_{h\max}$ for QCB is 20% lower than the SCB. However, the measured horizontal forces for both structures are close to each other (see figure 6). This inconsistence implies that the total wave force $F_{h\max}$ on the QCB attributes to not only the potential flow component F_{hW} but also the drag component F_{hD} due to wake effects. The length of structures in this study is smaller than the wave length ($\frac{R}{L_s}$ varies from 0.058 to 0.075, where R is the radius of the circular wall, L_s is the wave

length) and therefore a considerable wake effect is expected. Xie's study (2006) indicated that strong trailing vortices are formed on the leeside of submerged QCBs during the wave-structure interaction. QCBs are less streamlined than SCBs so that larger flow separations therefore drag are expected for QCBs. Thus it is important to include the drag component in the wave load calculation of QCBs and the following equation (8) instead of (7) should be used, even though the Keulegan-Carpenter number (KC) in this study varies from 1.59 to 2.40 indicating non-dominant drag component. We rewrite equation (2) to include the wake effects

$$F_{h\max} = (1+\lambda_D) F_{hW}, \tag{8}$$

where λ_D represents the fraction of the drag component in the maximum horizontal force, which is related to wave height (H_i), wave period (T_s), water depth (d) and structure geometry (e.g. shape and size). According to Qiu (1986), $\lambda_D \propto (KC) \cdot \frac{2kd + sinh2kd}{8sinh(2kd)tanh(kd)}$. Note that the flow velocity U is proportional to $\left(\frac{H_i}{T}\right)$ and KC is proportional to $\left(\frac{H_i}{R}\right)$. Furthermore, if we assume $d \cong R_c + H_i$ when a wave crest is passing over the structure (R_c is the crest freeboard height), we have $\frac{2kd + sinh2kd}{8sinh(2kd)tanh(kd)} \cong \frac{1}{8\pi}\frac{L_s}{d}$. As a result, we can give the expression of λ_D as

$$\lambda_D = a \cdot \left(\frac{H_i}{R}\frac{L_s}{d}\right) + b \tag{9}$$

By analyzing the measurements, we obtain a=-0.27 and b=1.60 for the QCB with a correlation coefficient close to 0.92 (see figure 9). The contribution of the drag component to the maximum horizontal force for the more streamlined SCB is negligible, i.e. λ_D =0 for the SCB.

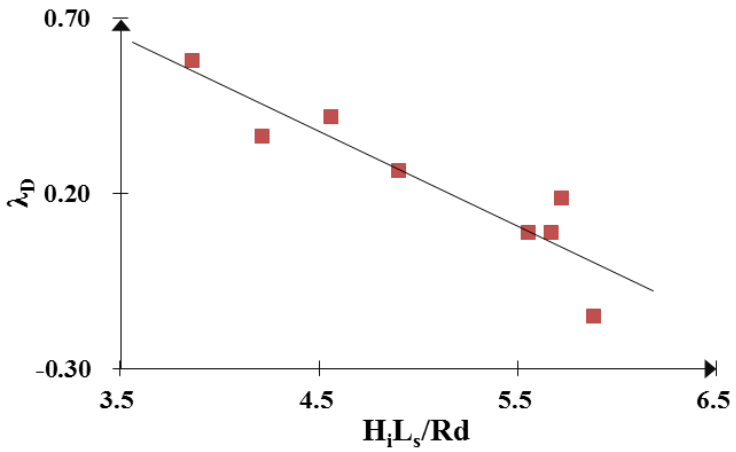

Figure 9. λ_D versus $\left(H_iL_s/Rd\right)$ for the quarter-circular breakwater.

We calculate the maximum horizontal forces ($F_{h\max}$) using equations (2) to (9) and compare with the measurements (see figure 10). The ratio of predictions to measurements has a mean value of 1.0 and standard deviations of 0.09 for the QCB and 0.13 for the SCB. Comparison of figure 10 with figure 6 suggests that the present model capture the observation better than Xie's (1999) model. In addition, the uncertainties in wave loading prediction (e.g. bias and spread) display a nearly normal stochastics in the present model and hence it is more suitable for a probabilistic design [Burcharth, 1999].

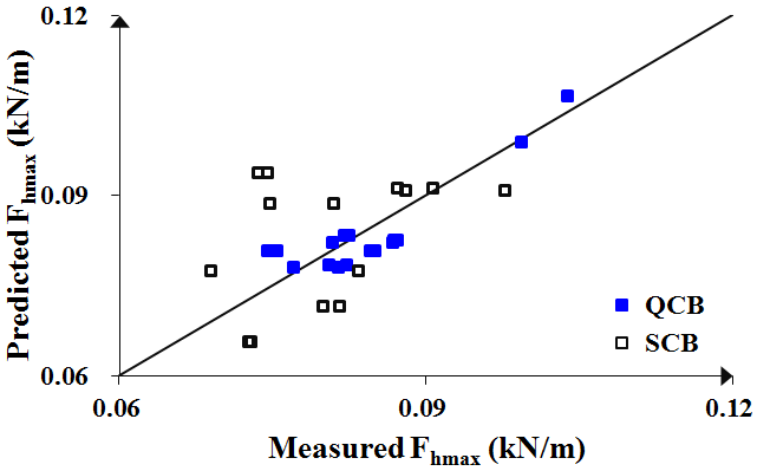

Figure 10. Comparison of the predicted maximum horizontal forces by the present wave load model equations (2)-(9) and measurements. The diagonal line denotes the prediction equal to the measurement.

6. Effect of wave transmission on dynamic pressure

As discussed previously, wave transmission affects the hydrodynamic loads on submerged SCBs and QCBs. In this section, we will explore the mechanism behind this based on the measured pressure distributions and the numerical results of vortex dynamics at the structure.

6.1. *Instantaneous pressure distribution*

The instantaneous pressure distribution along caisson at the time of the maximum horizontal force is shown in figure 11. The pressure at each pressure transducer for each run are first normalized using the toe pressure (p_b'), and then averaged over all runs. At the front wall, the pressure decreases from toe to crown due to phase shift and then becomes negative at the leeside corner. In general, the QCB has a slightly lower pressure over the front wall than the SCB. On the rear wall, the pressure has an approximately uniform distribution over the QCB while it increases from the crown to the mid-point and then decreases towards the bottom for the SCB. The magnitude of the leeside pressure on the QCB is smaller than that on the SCB and the difference becomes smaller towards the bottom. The negative pressure behind the crest of the breakwater in figure 11 is mainly due to the negative surface elevation displacement as indicated in figure 8. The wake effect may further modify the negative pressures on rear wall. The uplift pressure on the base slab increases linearly from the heel to the toe for both structures. The negative pressure at the heel can therefore be obtained through a linear extrapolation. In general, the heel pressure of emerged breakwaters is assumed to be zero in the design of emerged breakwaters. Therefore, the submerged circular-front breakwaters may have a lower uplift force than emerged vertical breakwaters. Goda [2010] also came to the same conclusion that a very small freeboard will result in a reduced uplift pressure due to wave overtopping.

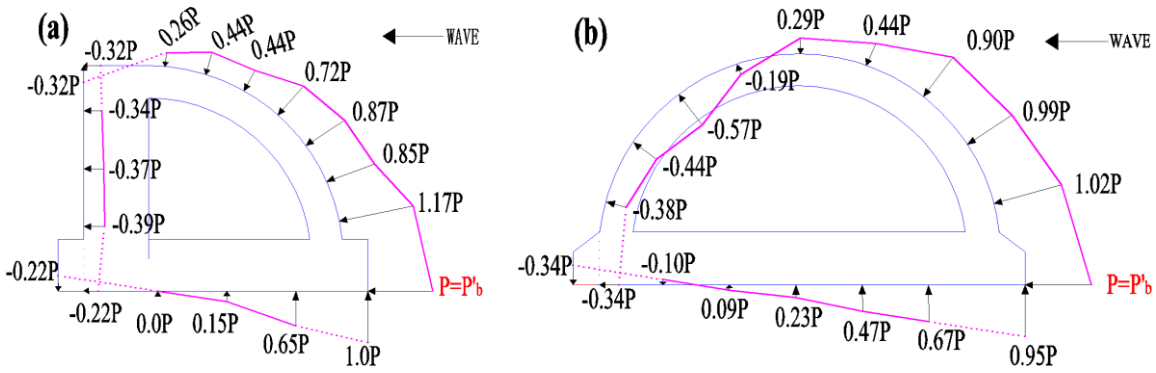

Figure 11. Instantaneous pressure distribution at the time of the peak horizontal force: (a) for the quarter-circular breakwater; (b) for the semicircular breakwater. The dotted line indicates a linear extrapolation from the measurements.

6.2. *Effect of flow disturbance*

The difference between wave loads on submerged SCBs and QCBs mainly comes from the difference in the pressure on the leeside wall. Compared with semicircular and vertical breakwaters, the quarter-circular breakwater has asymmetry geometry. Hur et al. [2004] concluded that a complicated vortex generated by structural asymmetry greatly affects the time variation of the transverse wave force exerted on an asymmetric structure.

A numerical wave flume is developed in this section to examine the effect of vortex dynamics on pressure. This numerical flume is based on a free surface flow model developed by Lin & Liu [1998]. In this model, the motion of an incompressible fluid is described by the 2D Reynolds-Averaged-Navier-Stokes equations (RANS) along with a nonlinear $k-\varepsilon$ turbulent model (see Appendix B.). The spatially averaged Navier-Stokes equations are used to describe the mean motion of flow in porous media by including additional frictional forces [Lin and Karunarathna, 2007]. Finite difference method is used for discretization, in which the advection terms are discretized with a mixed upwind and central difference scheme while the dissipation terms are discretized with a central difference scheme. A two-step projection algorithm is adopted to obtain the flow fields, pressures, and turbulence parameters. The volume of fluid function (VOF) by Hirt and Nichols [1981] is used to track the free surface displacement. This type of approach has been used extensively to study surf zone problems such as wave breaking

(Lubin et al 2003; Zhao et al 2004; Christensen, E.D., 2006; Wang et al 2009; Zhang et al 2009, Bakhtyar et al 2010 and 2012, Xie 2012).

This model has been applied widely to wave-structure interaction problems. Examples include the wave interaction with composite porous structures [Liu et al., 1999], with a rectangular obstacles [Lin, 2004], wave overtopping over a smooth impermeable seawall [Reeve et al., 2008], over rubble mound breakwaters [Losada et al., 2008], and over a seaward sloping dike [Peng and Zou, 2011], wave transformation over circular breakwaters [Jiang et al., 2008], over vertical breakwaters [Jiang et al., 2010], and over a low-crested structure [Zou and Peng, 2011].

In this study, the numerical flume is set up following the experiment configuration in figure 2. The combination of second-order polynomial function and sinusoidal function is employed to construct the structure boundary in the model. The partial cell technique is used to simplify the treatment of internal obstacles and solid boundaries [Lin, 2007 2008]. In this method, an openness function (β) is introduced to represent the ratio of the fluid-occupied volume to total volume of a computation cell. As a result, the whole computational domain is divided into fluid cells (β =1), solid cells (β =0) and partial cells ($0<\beta<1$). The mean value of a variable for a particular cell in the model is defined as the product of the value of openness function and the variable in that cell. Since the grid resolution used in the model is not fine enough to resolve the viscous boundary layer at the solid boundary, free slip boundary conditions are applied at the solid boundary to avoid underestimating flow velocity there. The pressure variation across the thin viscous boundary layer adjacent to a solid boundary is negligible [Zou, 1998, 2002] and the pressure boundary condition $\partial p/\partial n=0$ is often imposed on the solid boundary in the immersed boundary method [Zhang et al., 2010]. Thus the free slip boundary condition has little effect on the model results of wave loading on the breakwater while avoiding using excessive CPU time to resolve the very thin viscous boundary layers. A combination of zero-pressure and zero normal gradient of mean tangential velocity is imposed on the free surface. The turbulent kinetic energy (k) and the dissipation rate (ε) are assumed to be a function of frictional velocity at grid points immediately adjacent to the solid boundaries and have a zero normal gradient on the free surface. An open boundary condition is applied at the inlet and outlet boundaries. An internal wave-maker

developed by Lin and Liu (1999) is used to generate irregular waves in the numerical flume. The inverse Fourier transformation is first used to decompose a specific JONSWAP spectrum into wave components. Then, an irregular wave train is reconstructed by adding a mass source function in the equation of mass conservation in a source region. The mass source function is the summation of the different wave components. The source region is a rectangle with the size of 0.05m (width) $\times$ 0.14m (height). The source region is located 1.5m away from the inlet boundary and is 0.22m below the still water level. A non-uniform mesh was used in this study with the cell size from 0.001m near the solid boundaries to 0.01m away from the structures in both x- and z-directions.

As shown in figure 12 (a) and (b), the predicted and measured significant wave height agree well with each other. The significant wave heights display a mild increase between the first and fourth gauge stations. Then, the significant wave height is reduced considerably between the fourth and fifth gauge stations due to wave breaking over the submerged structure. In figure 12 (c), the good agreement between the predicted and measured wave spectra demonstrates that the incident wave spectrum is reproduced well in the numerical flume. In figure 12 (d), the predicted and measured maximum horizontal forces are normalized by $\gamma_w H_i h_c$, where γ_w is the specific weight of water, H_i the incident wave height, and h_c the caisson height. The mean ratio of prediction to measurement is 1.01 for the QCB and 1.04 for the SCB. The standard deviation of the ratio is 0.17 for the QCB and 0.07 for the SCB. The deviation between the predicted and observed wave loads in figure 12 (d) is partly due to the deviation between predicted and observed incident wave spectra in figure 12 (c). The larger scatter in the case of QCB may be caused by stronger flow separation and vortices behind the structure.

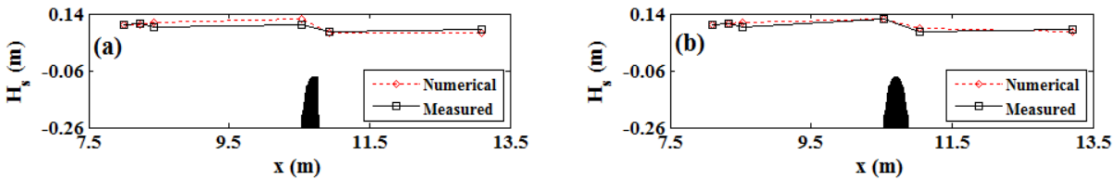

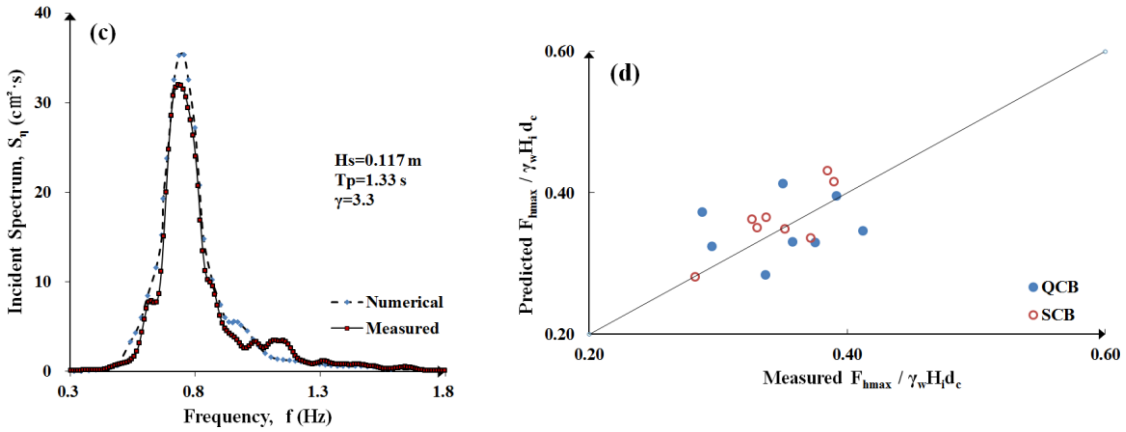

Figure 12. Comparison of the predicted and measured significant wave heights at six gauge stations indicated in figure 2 for test 6 (a) the quarter-circular breakwater, (b) the semicircular breakwater; (c) incident wave spectrum for test 1; (d) dimensionless maximum horizontal forces for the QCB and the SCB.

Regular waves are used next in the simulation to explore the relationship between the wave load and vorticity. Figure 13 (a) and (b) demonstrate that both QCB and SCB have similar flow pattern before the crown of the caisson. After the crown, the flow is smooth for the SCB but with an obvious trailing vortex present for the QCB. Figure 13 (c) and (d) show that both structures have an identical interaction between the vorticity and the wave force at point 1 but a great difference at point 2. At point 2, the submerged QCB displays a greater scatter than the submerged SCB due to larger variation in the vorticity. At point 3, the magnitude of the vorticity for both structures is small. As indicated in Chang et al. (2005), the rotational flow is confined to the region about 2 times wave particle excursion from a submerged obstacle and the center of the downstream vortices is located at about half of wave particle excursion away from the leeside corner. In our study, the wave particle excursion is between 4.7 cm and 7.0 cm, and the distance between point 3 and the leeside corner is 13.5 cm that reaches the edge of the rotational flow. The QCB has a greater vorticity than the SCB at point 3 that attributes to stronger vortex diffusion. Figure 13 (e) and (f) illustrate the variation of pressure with vorticity at point 2. The pressure has a similar fluctuation period to the vorticity but a phase lag to the latter. It also reveals the structural asymmetry at the QCB generates a larger variation in the

vorticity, which considerably affects the magnitude and phase of the pressure on the structure.

(a)

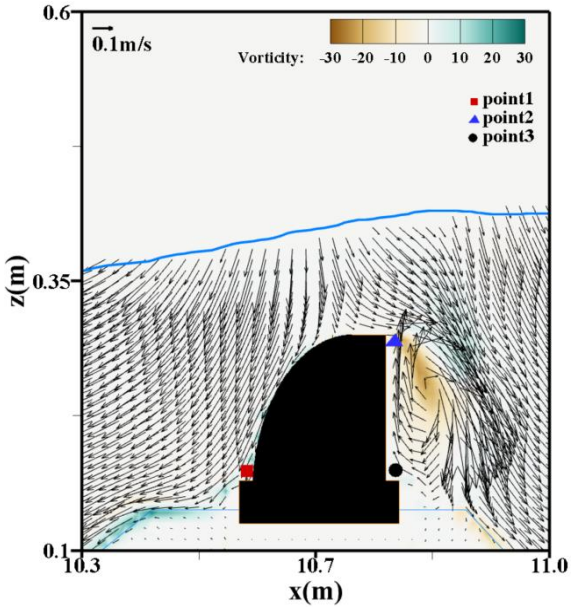

(b)

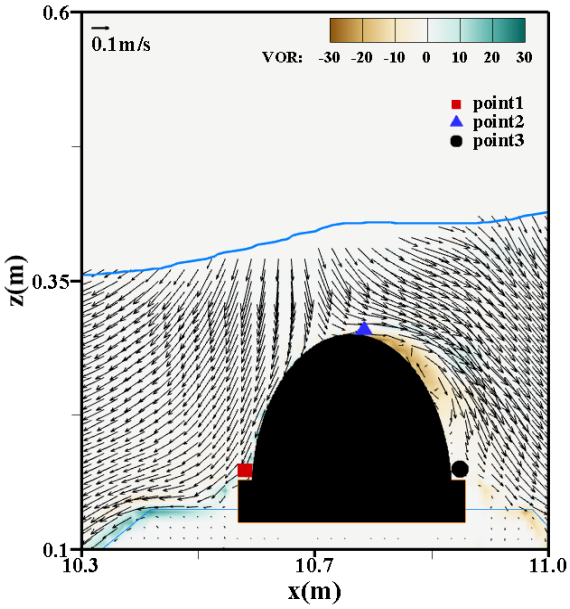

(c)

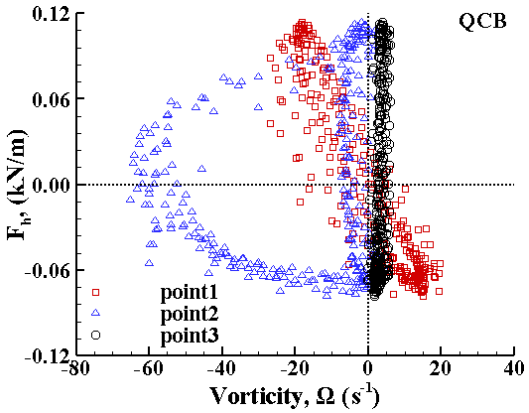

(d)

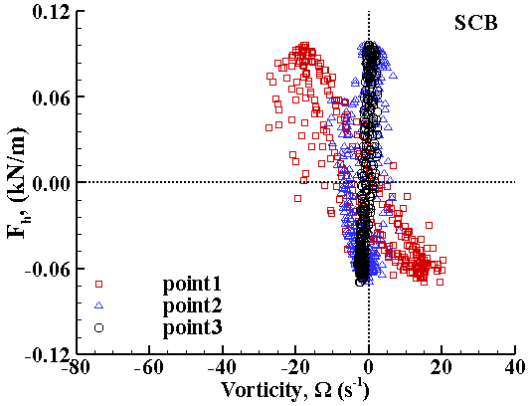

(e)

(f)

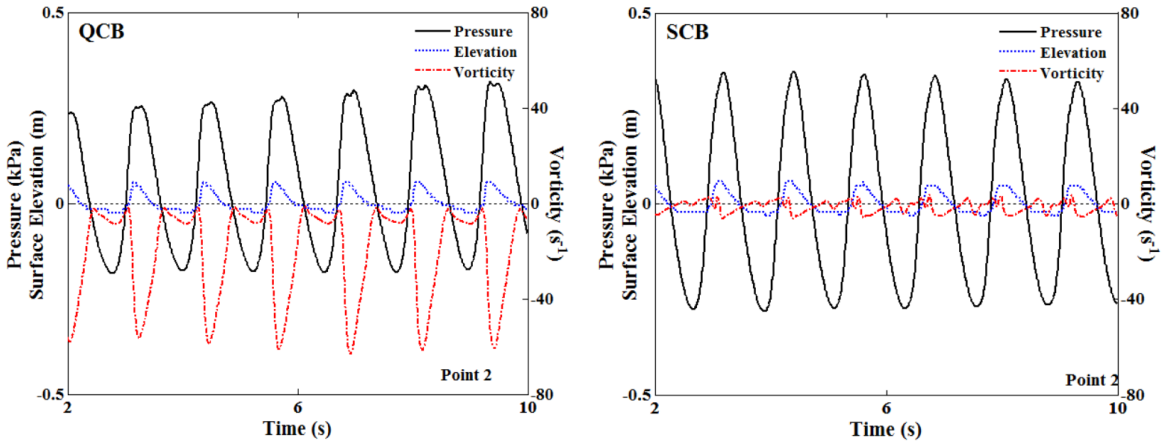

Figure 13. Variations of velocity, force and pressure due to regular waves ($d = 0.383\ m$, $H = 0.117\ m$, $T = 1.24\ s$): (a) and (b) flow fields, vorticity (color bar) and surface elevation; (c) and (d) total horizontal force as a function of vorticity at point 1, 2 and 3 indicated in (a) and (b); (e) and (f) time series of surface elevation, pressure and vorticity at point 2 near the crest of the caisson.

7. Conclusions

In this study, the characteristics of the wave loads acting on submerged semi--and quarter-circular breakwaters under irregular waves have been investigated. The main conclusions can be summarized as follows.

Submerged semi- and quarter-circular breakwaters have a similar anti-sliding response and wave force spectra. Comparison with previous observations indicates that the normalized wave force on submerged circular-front breakwaters under irregular waves is less than that under regular waves.

Xie's model gives a conservative estimation of the wave loads on submerged circular-front breakwaters. We improve the model by including the effect of wave transmission on the pressures on submerged circular structures.

The instantaneous pressures at the time of the maximum horizontal force for both semi- and quarter-circular breakwaters exhibit the same behaviors on the front wall but great differences on the rear wall due to distinct wake behaviors behind structures. RANS-VOF modeling results show that wave-induced vortices have a considerable effect on the wave loads of the quarter-circular breakwater but not the semicircular breakwater.

The wave load model was further improved by incorporating the effect of flow separation and vorticity due to wave transmission.

According to Sasajima et al. [1994], the semicircular breakwaters are categorized as impermeable type, front dissipating type (seaside wall perforated), rear dissipating type (leeside wall perforated) and fully dissipating type (both seaside and leeside walls perforated). As reviewed in Dhinakaran et al. [2012], a submerged perforated quartercircular and semicircular structure with a suitable permeability is subject to a smaller wave load than an impermeable breakwater with the same geometry. The reduction in the wave loading is due to wave energy loss to generate the turbulent flow within the hollow chamber. The amount of reduction is worth further investigation. However, the present study of impermeable breakwater provides a benchmark for both types of breakwater.

The behaviors of vortices are controlled by many factors, for example, the geometry and permeability of a structure, the ratio of structure dimension over wavelength, the relative freeboard height, wave height, and wave period. Further study is required to understand the relationship between vorticity and pressure for submerged structures, which will lead to great improvement of the formulas calculating wave loads on submerged obstacles.

Acknowledgements

The first author acknowledges the support of the Open Fund of State Key Laboratory of Hydraulic Engineering Simulation and Safety from Tianjin University (HESS-1310), the Natural Science Foundation of Tianjin (14JCYBJC22100) and the National Natural Science Foundation of China (51509177), the State Scholarship Fund (201308120008 During the course of this work, the second author was supported by the Physical Oceanography Program of National Science Foundation under Award Number 1436642, the Maine Sea Grant and NOAA through a grant (NA10OAR4170072), the Ensemble Estimation of Flood Risk in A Changing Climate (EFRaCC) project funded by the British Council under its Global Innovation Initiative and the open fund of the State Key Laboratory of Hydraulics and Mountain River (SKHL) at Sichuan University. The authors are grateful to Professor Pengzhi Lin from Sichuan University, who generously supplied his RANS-VOF code for the present work, and to Dr. Zhong Peng at Fugro GEOS Ltd. for helpful discussions.

Appendix A: The wave load formula for submerged semicircular breakwaters by Xie (1999).

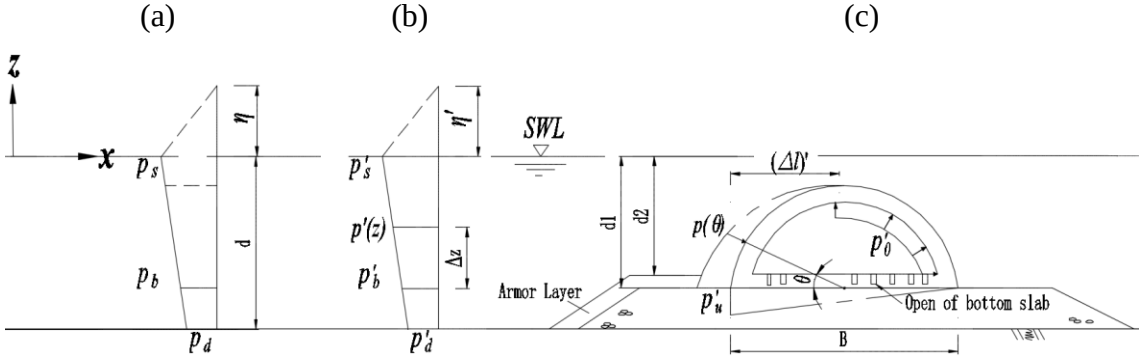

Figure A-1. Sketch of wave load model for submerged semicircular breakwater: (a) pressures on a fictional upright section; (b) pressures after phase correction; (c) pressures after center angle correction.

$$\eta' = \eta = 0.75(1+\cos\beta)H_i \tag{A.1}$$

$$p_s^{'} = p_s = 0.5(1+\cos\beta)\left(\alpha_1+\alpha_2\cos^2\beta\right)\gamma_w H_i \tag{A.2}$$

$$p_b' = \lambda_p' p_b = \lambda_p' \alpha_3 p_s^{'}; \lambda_p' = \cos\left[\frac{2\pi(\Delta l)'}{L}\right] \tag{A.3}$$

$$p'(z) = p_b' + (p_s' - p_b')\cdot z/d_1 \tag{A.4}$$

$$p'(\theta) = p'(z)\cos(\theta) \tag{A.5}$$

$$p_u' = \begin{cases} p_b', \ for \quad \varepsilon_b < 0.1 \\ 0, \quad for \quad \varepsilon_b \geq 0.1 \end{cases} \tag{A.6}$$

$$p_0' = \begin{cases} 0, for \quad \varepsilon_b < 0.1 \\ p_b'/2, \quad for \quad \varepsilon_b \geq 0.1 \end{cases} \tag{A.7}$$

$$\alpha_1 = 0.6 + 0.5\left[\frac{4\pi d/L}{\sinh(4\pi d/L)}\right]^2, \qquad \alpha_2 = \min\left\{\frac{h_b - d_2}{3h_b}\left(\frac{H}{d_2}\right)^2, \frac{2d_2}{H}\right\}, \qquad \alpha_3 = 1 - \frac{d_1}{d}\left[1 - \frac{1}{\cosh(2\pi d/L)}\right]$$

Where

η and η' elevation of zero dynamic pressure point above the still water level (m).

β angle between the wave direction and the normal vector of structure

surface (°).

H_i	incident wave height (m, $H_{1\%}$ for irregular waves).
L	incident wavelength (m, the significant wavelength L_s for irregular waves).
d	water depth in front of breakwater (m).
d_1	water depth above wall bottom (m).
d_2	water depth above armor layer (m).
h_b	water depth at the location at a distance $5H_{1/3}$ seaward of the breakwater (m).
γ_w	water density (kN/m^3).
p_s' and p_s	pressure at the still wave level (kpa).
p_b' and p_b	pressure at the bottom level of caisson (kpa).
$p'(z)$	pressure at the water depth of $d_1 - z$ (kpa).
$p(\theta)$	pressure after angle correction to $p'(z)$ (kpa); θ is the central angle at the acting point (°).
p_u'	wave uplift pressure at the toe of caisson (kpa).
p_0'	pressure on the inside circumference of rear circular wall (kpa).
ε_b	opening ratio of bottom slab.
$(\Delta l)'$	horizontal distance between the toe and the crown (m).
λ_p'	phase correction coefficient (m).
α_1	coefficient representing the variation of pressure with the wave period.
α_2	coefficient representing the variation of pressure with the height of the rubble mound.
α_3	coefficient representing a linear relationship between p_s' and p_d'.

For $R/L \le 0.085$ only, where R is the radius of circular wall.

Appendix B: Reynolds Averaged Navier-Stokes equations with nonlinear turbulent kinetic-dissipation equations.

Continuity equation

$$\frac{\partial \bar{u}}{\partial x}+\frac{\partial \bar{w}}{\partial z}=0 \tag{B.1}$$

Momentum equations

$$\frac{\partial \bar{u}}{\partial t}+\bar{u}\frac{\partial \bar{u}}{\partial x}+\bar{w}\frac{\partial \bar{u}}{\partial z}=-\frac{1}{\rho}\frac{\partial \bar{p}}{\partial x}+\frac{\partial}{\partial x}\left(\nu\frac{\partial \bar{u}}{\partial x}\right)+\frac{\partial}{\partial z}\left(\nu\frac{\partial \bar{u}}{\partial z}\right)-\frac{\partial}{\partial x}\langle u'u'\rangle-\frac{\partial}{\partial z}\langle u'w'\rangle \tag{B.2}$$

$$\frac{\partial \bar{w}}{\partial t}+\bar{u}\frac{\partial \bar{w}}{\partial x}+\bar{w}\frac{\partial \bar{w}}{\partial z}=-\frac{1}{\rho}\frac{\partial \bar{p}}{\partial z}+\frac{\partial}{\partial x}\left(\nu\frac{\partial \bar{w}}{\partial x}\right)+\frac{\partial}{\partial z}\left(\nu\frac{\partial \bar{w}}{\partial z}\right)-\frac{\partial}{\partial x}\langle u'w'\rangle-\frac{\partial}{\partial z}\langle w'w'\rangle-g \tag{B.3}$$

Turbulent kinetic energy equation

$$\frac{\partial k}{\partial t}+\bar{u}\frac{\partial k}{\partial x}+\bar{w}\frac{\partial k}{\partial z}=\frac{\partial}{\partial x}\left[\left(\nu+\frac{\nu_t}{\sigma_k}\right)\frac{\partial k}{\partial x}\right]+\frac{\partial}{\partial z}\left[\left(\nu+\frac{\nu_t}{\sigma_k}\right)\frac{\partial k}{\partial z}\right]-\langle u'u'\rangle\frac{\partial \bar{u}}{\partial x}-\langle u'w'\rangle\frac{\partial \bar{u}}{\partial z}-\langle u'w'\rangle\frac{\partial \bar{w}}{\partial x}-\langle w'w'\rangle\frac{\partial \bar{w}}{\partial z}-\varepsilon \tag{B.4}$$

Energy dissipation equation

$$\frac{\partial \varepsilon}{\partial t}+\bar{u}\frac{\partial \varepsilon}{\partial x}+\bar{w}\frac{\partial \varepsilon}{\partial z}=\frac{\partial}{\partial x}\left[\left(\nu+\frac{\nu_t}{\sigma_\varepsilon}\right)\frac{\partial \varepsilon}{\partial x}\right]+\frac{\partial}{\partial z}\left[\left(\nu+\frac{\nu_t}{\sigma_\varepsilon}\right)\frac{\partial \varepsilon}{\partial z}\right]-C_{\varepsilon 1}\frac{\varepsilon}{k}\langle u'u'\rangle\frac{\partial \bar{u}}{\partial x}-C_{\varepsilon 1}\frac{\varepsilon}{k}\langle u'w'\rangle\frac{\partial \bar{u}}{\partial z}-C_{\varepsilon 1}\frac{\varepsilon}{k}\langle u'w'\rangle\frac{\partial \bar{w}}{\partial x}-C_{\varepsilon 1}\frac{\varepsilon}{k}\langle w'w'\rangle\frac{\partial \bar{w}}{\partial z}-C_{\varepsilon 2}\frac{\varepsilon^2}{k} \tag{B.5}$$

where

x and z	Cartesian coordinates (m) in horizontal and vertical direction.
t	Time (s).
$\bar{u}$ and $\bar{w}$	mean velocity components in x- and z-directions (m/s).
$\bar{P}$	mean pressure (kPa).
ρ	fluid density (kg/m^3).
g	gravitational acceleration (m/s^{-2}).
ν_t	eddy viscosity, $\nu_t = C_d\frac{k^2}{\varepsilon}$.
ν	kinematic viscosity, $\nu = 1.3\times10^{-6}\ m^2/s$.
$\langle u'u'\rangle, \langle u'w'\rangle, \langle w'w'\rangle$	Reynolds stresses.
k	turbulent kinetic energy (kJ).
ε	energy dissipation rate.
Constants	σ_k=1.0, σ_ε=1.3, C_d=0.09, $C_{\varepsilon 1}$=1.44, $C_{\varepsilon 2}$=1.92.

References

Bakhtyar, R., Razmi, A.M., Barry, D.A., Yeganeh-Bakhtiary, A. & Q.-P. Zou, 2010. Air-water two-phase flow modeling of turbulent surf and swash zone wave motions. *Advances in Water Resources*, 33(12), 1560-1574.

Blackmore, P.A. and Hewson, P.J., 1984. Experiments on full-scale wave impact pressures. *Coast. Eng.* 8(4), 331-346.

Bullock, G.N., Crawford, A.R., Hewson, P.J., Walkden, M.J.D. and Bird, P.A.D., 2001. The influence of air and scale on wave impact pressures. *Coast. Eng.* 42(4), 291-312.

Bullock, G.N., Obhrai, Peregrine, D.H. Bredmose, H., 2007. Violent breaking wave impacts. Part 1: Results from large-scale regular wave tests on vertical and sloping walls. *Coast. Eng.* 54, 602-617.

Burcharth, H. F., Kramer, M., Lamberti, A. and Zanuttigh, B., 2006. Structural stability of detached low crested breakwaters. *Coast. Eng.* 53(4), 381-394.

Burcharth, H.F. and Sorensen, J.D., 1999. Design of vertical wall caisson breakwaters using partial safety factors. *Coast. Eng. 1998* (Vols 1-3), 2138-2151.

Chang, K.A., Hsu, T.J. and Liu, P.L.F., 2005. Vortex generation and evolution in water waves propagating over a submerged rectangular obstacle. Part II: Cnoidal waves. *Coast. Eng.* 52, 257-283.

China Communications Construction Company First Harbor Consultants Co., Ltd., 2011. *Code of Design and Construction of Breakwaters (CDCB)*. China Communications Press (Beijing, China). (In Chinese)

Christensen, E.D., 2006. Large eddy simulation of spilling and plunging breakers. Coastal Engineering 53 (5–6), 463–485

Cooker, M.J., Peregrine, D.H., 1992. Wave impact pressures and its effect upon bodies lying on the seabed. *Coast. Eng.* 18(3-4), 205-229.

Cuomo, G., Lupoid, G., Shimosako, K. and Takahashi, S., 2011. Dynamic response and sliding distance of composite breakwaters under breaking and non-breaking wave attack. *Coast. Eng.*, 58(10), 953-969.

Dean, R.G. and Dalrymple, R.A., 1991. *Water Wave mechanics for engineers and scientists.* World Scientific, pp. 213.

Dhinakaran, G., Sundar, V., Sundaravadivelu, R. and Graw K.U., 2009. Effect of perforations and rubble mound height on wave transformation characteristics of emerged semicircular breakwaters. *Ocean Eng.* 36 (15-16), 1182-1198.

Dhinakaran, G., Sundar, V. and Sundaravadivelu, R., 2012. Review of the research on emerged and submerged semicircular breakwaters. Proc. of the Institution of Mechanical Engineers, Part M: *J. Eng. for the Maritime Environment* 226(4), 397-409.

Ergin, A. and Abdalla, S., 1993. A comparison study on breaking wave forces on vertical walls. *J. Waterway, Port, Coast. and Ocean Eng.*, ASCE 115(1), 58-65.

Franco L., 1994. Vertical breakwaters: the Italian experience. *Coast. Eng.* 22, 31-55.

Goda, Y., 1970. *Numerical experiments on wave statistics with spectral simulation.* Rept. Port and Harbour Res. Inst. 9 (3), pp. 3-57.

Goda, Y., 2010. *Random Seas and Design of Maritime Structures*. World Scientific. (5 Toh Tuck Link, Singapore).

Goda, Y. and Takagi, H., 2000. A reliability design method of caisson breakwaters with optimal wave heights. *Coast. Eng. J.* 42(4), 357-387.

Gotoh, H., Okayasu, A. and Watanabe, Y., 2013. *Computational Wave Dynamics (Advanced Series on Ocean Engineering 37)*. World Scientific Publishing Co. Pte. Ltd., Singapore, pp. 1-44.

Hattori, M., Arami, A. and Yui, T., 1994. Wave impact pressure on vertical walls under breaking waves of various types. *Coast. Eng.* 22(1-2), 79-114.

Hirt, C.W. and Nichols, B.D., 1981. Volume of fluid (VOF) method for the dynamics of free boundaries. *J. Computational Physics*, 39, 201-225.

Hur, D-S., Mizutani, N. and Kim, D-S., 2004. Direct 3-D numerical simulation of wave forces on asymmetric structures. *Coast. Eng.* 51, 407-420.

Jeng, D.-S., Ye, J.-H., Zhang, J.-S. and Liu, P.L.-F., 2013. An integrated model for the wave-induced seabed response around marine structures: Model verifications and applications. *Coast. Eng.* 72, 1-19.

Jiang, X.L., Gu, H.B. and Li, Y.B., 2008. Numerical simulation on hydraulic performances of quarter circular breakwater. *China Ocean Eng.* 22(4), 585-594.

Jiang, X.L., Wu, M.L. and Li, Y.B., 2010. Study on the flow field around vertical breakwater under different overtopping conditions based on numerical simulation. *China Ocean Eng.* 24(4), 641-651.

Jiang, X.L., Guo, S.L. and Li, Y.B., 2012. Study on hydraulics and wave energy dissipation as wave passing circular breakwater. *The Ocean Eng.* 30(3), 59-67. (In Chinese)

Johnson, H.K., 2006. Wave modeling in the vicinity of submerged breakwaters. *Coast. Eng.* 53, 39-48.

Kirkgöz, M.S., 1982. Shock pressures of breaking wave on vertical walls. *Journal of Waterway, Harbours and Coastal Engineering Division*, ASCE 108, 87-103.

Kirkgöz, M.S., 1992. Influence of water depth on the breaking wave impact on vertical and sloping walls. *Coast. Eng.* 18, 297-314.

Kobayashi, N., Leslie, E.M., Takao, O. and Melby, J., 2007. Irregular breaking wave transmission over submerged porous breakwater. *J. Waterway, Port, Coast. and Ocean Eng.*, ASCE 133(2), 104-116.

Li, Y.B., Ma, Q.H. and Gu, H.B., 2003. Study about several methods of calculation of wave forces on semi-circular breakwaters. *Port Eng. Technology* 2, 1-5.

Li, Y.B., Jiang, X.L. and Liu R., 2006. Discussion on the relationship between characteristics and the reasons of breakwater failures. *The Ocean Eng.* 24(2), 130-138.

Lin, P.Z., 2004. A numerical study of solitary wave interaction with rectangular obstacles. *Coast. Eng.* 51, 35-51.

Lin, P.Z. and Liu, P.L.-F. 1998. A numerical study of breaking waves in the surf zone. *J. Fluid Mech.* 359, 239-264.

Lin, P.Z. and Liu, P.L.-F. 1999. Internal wave-maker for Navier-Stokes equations models. *J. Waterway, Port, Coast. and Ocean Eng.* 125(4), 207-215.

Lin, P.Z. and Anuja Karunarathna, S.A.S., 2007. Numerical study of solitary wave interaction with porous breakwaters. *J. Waterw. Port Coast. Ocean Eng.* 133 (5), 352-363.

Lin, P.Z., 2007. A fixed-grid model for simulation of a moving body in free surface flows. Computers & Fluids, 36: 549-561.

Lin, P.Z., 2008. *Numerical Modeling of Water Waves*. CRC Press, Taylor & Francis Co.

Liu, P.L.-F., Lin, P., Chang, K.-A. and Sakakiyama, T., 1999. Numerical modeling of wave interaction with porous structures. *J. Waterw. Port Coast. Ocean Eng.* 125(6), 322-330.

Liu, Y. and Li, H.J., 2012. Analysis of wave interaction with submerged perforated semi-circular breakwaters through multipole method. *Applied Ocean Research*, 34,164-172.

Liu, Y. and Li, H. J., 2013. Analysis of oblique wave interaction with a submerged perforated semicircular breakwater. *J. Eng. Math*. 83, 23-36.

Liu, Y.H., Wu, Y.Q. and Li, Y.B., 2006. Model experiment on hydraulic characteristics of quartercircular breakwater. *Ocean Technology* 25(2), 94-98. (In Chinese)

Losada, I.J., Lara, J.L., Guanche, R. and Gonzalez-Ondina, J.M., 2008. Numerical analysis of wave overtopping of rubble mound breakwaters. *Coastal Eng.* 55(1), 47-62.

Lubin, P., Vincent, S., Abadie, S., and Caltagirone, J. P., 2006. Three-dimensional large eddy simulation of air entrainment under plunging breaking waves, Coastal Engineering. 53, 631-635.

Mansard, E.P.D. and Funke, E.R., 1980. The measurement of incident and reflected spectra using a least square method. *Proc. of the 17th ICCE*, ASCE 1, 154-172.

Mizutani, N., Mostafa, A.M. and Iwata, K., 1998. Nonlinear regular wave, submerged breakwater and seabed dynamic interaction. *Coast. Eng.* 33, 177-202.

Oumeraci, H., 1994. Review and analysis of vertical breakwater failures - lessons learned. *Coast. Eng.* 22, 3-29.

Oumeraci, H., Kortenhaus, A., Allsop, W., Groot, M.D., Crouch, R., Vrijling, H., and Voortman, H., 2001. *Probabilistic Design Tools for Vertical Breakwaters*. ed. Kortenhaus, A. and Voortman, H. (Balkema, Lisse, Rotterdam, The Netherlands), pp. 225-260.

Peng Z. and Zou Q.-P., 2011. Spatial distribution of wave overtopping water behind coastal structures. *Coastal Eng.* 58, 489-498.

Polyanin, A.D. and Manzhirov, A.V., 1998. *Handbook of integral equations (8.7-1. Quadrature Formulas)*. CRC Press (Boca Raton, USA).

Poupardin, A., Perret, G., Pinon, G., Bourneton, N., Rivoalen, E. and Brossard J., 2012. Vortex kinematic around a submerged plate under water waves. Part I: Experimental analysis. *European J. of Mech. B/Fluids* 34, 47-55.

Prabhakar, V. and Sundar, V., 2001. Standing wave pressure on walls. *Ocean Eng.* 28, 439-455.

Rambabu, A.C., Mani, J.S., 2005. Numerical prediction of performance of submerged breakwaters. *Ocean Eng.* 32, 1235-1246.

Rao, Y.H., Yu, Y.X. and Zhang, N.C., 2001. Hydraulic experimental study on submerged semicircular breakwaters. *ACTA OCEANOLOGICA SINICA* 23(2), 124-131. (In Chinese)

Reeve, D.E., Soliman, A. and Lin, P.Z., 2008. Numerical study of combined overflow and wave overtopping over a smooth impermeable seawall. *Coastal Eng.* 55(2), 155-166.

Qiu, D.H., 1986. *Wave theory and its application in Engineering*. High Education Press (Beijing, China). (In Chinese)

Sasajima, H., Koizuka, T. and Sasayama, H., 1994. Field demonstration test on a semicircular breakwater. *HYDROPORT'94*, Yokosuka, Japan 1, 593-615.

Shi, Y.J., Wu, M.L., Jiang, X.L. and Li Y.B., 2011. Experimental researches on reflective and transmitting performances of quarter circular breakwater under regular and irregular waves. *China Ocean Eng.* 25(3), 469-478.

Sundar, V. and Ragu, D., 1997. Wave induced pressures on semicircular breakwaters. *2nd Indian national conference on harbour and ocean engineering*, Thiruvananthapuram, Kerala, India, 278-287.

Sundar, V. and Ragu, D., 1998. Dynamic pressures and run-up on semicircular breakwaters due to random waves. *Ocean Eng.* 25(2-3), 221-241.

Takahashi, S., Shimosako, K., Kimura, K., and Suzuki, K., 2001. Typical Failures of Composite Breakwaters in Japan. *Coast. Eng. 2000*, 1899-1910.

Tanimoto, K., Yoshinoto, N., Namerikawa, N. and Ishimaru, Y., 1987. Hydraulic characteristics and design wave forces of semicircular caisson breakwaters. *Coast. Eng. (JSCE)* 34, 551-555. (In Japanese)

Tanimoto, K. and Takahashi, S., 1994. Japanese experience on composite breakwaters. *International workshop on wave barriers in deep waters*, Yokosuka, Japan, Nagase, Port and Harbor Research Institute, 1-24.

van der Meer, J.W., Briganti, R., Zanuttigh, B. and Wang, B., 2005. Wave transmission and reflection at low-crested structures: Design formulae, oblique wave attack and spectral change. *Coast. Eng.* 52(10-11), 915-929.

Wang, Z. Y., Zou Q. P. and Reeve D. E., 2009 a. Simulation of spilling breaking waves using a two phase flow CFD model, Computers & Fluids 38 (10), 1995-2005.

Xie, S.L., 1999. Wave forces on submerged semicircular breakwater and similar structures. *China Ocean Eng.* 13(11), 63-72.

Xie, S.L., Li, Y.B., Wu, Y.Q. and Gu, H.B., 2006. Preliminary research on wave forces on quarter circular breakwater. *The Ocean Eng.* 24(1), 14-18. (In Chinese)

Xie, Z., 2012. Numerical study of breaking waves by a two-phase flow model, Int. J. Numer. Methods Fluids 70, 246–268.

Young, D.M. and Testik, F.Y., 2009. Onshore scour characteristics around submerged vertical and semicircular breakwaters. *Coast. Eng.* 56(8), 868-875.

Young, D.M. and Testik, F.Y., 2011. Wave reflection by submerged vertical and semicircular breakwaters. *Ocean Eng.* 38, 1269-1276.

Yu, Y.X., Zhang, N.C. and Rao, Y.H., 1999. Hydraulic experimental study on semicircular breakwaters. *The Ocean Eng.* 17(4), 39-48. (In Chinese)

Yuan, D.K. and Tao, J.H., 2003. Wave forces on submerged, alternately submerged, emerged semicircular breakwater. *Coast. Eng.* 48(2), 75-93.

Zhang, N.C., Wang, L.Q. and Yu, Y.X., 2005. Oblique irregular waves load on semicircular breakwater. *Coast. Eng. J.* 47(4), 183-204.

Zhang, Y.L., Zou, Q.-P., Greaves, D., Reeve, D., Hunt-Raby, A., Graham, D., James, P. and Lv, X., 2010. A level set immersed boundary method for water entry and exit. *Communications in Computational Physics*, 8(2), 265-288.

Zhao, Q., Armfield S., Tanimoto K. 2004. Numerical simulation of breaking waves by a multi-scale turbulence model. Coastal Engineering, 51(1),53–80.

Zou, Q.-P., 1998. A viscoelastic model for turbulent flow over an undulating topography. *J. Fluid Mech.* 355, 81-112.

Zou, Q.-P., 2002. An analytical model of wave bottom boundary layers incorporating turbulent relaxation and diffusion effects. *J. Phys. Oceanogr*. 32(9), 2441-2456.

Zou, Q.-P. and Peng, Z., 2011. Evolution of wave shape over a low-crested structure. *Coast. Eng.* 58(6), 478-488.